ANALYSIS OF LAMINAR FORCED CONVECTION INSIDE A SQUARE VENTILATED CAVITY USING THE OPENFOAM®

P. C. Mioralli[a], V. L. Scalon[b], E. Avallone[a], and S. A. Verdério Júnior[c]

[a,c]Instituto Federal de São Paulo - IFSP
Departamento de Indústria
[a]CEP 15808-305, Catanduva, SP, Brasil
[c]CEP. 14801-600, Araraquara, SP, Brasil
mioralli@ ifsp.edu.br
[b]Universidade Estadual Paulista
"Júlio de Mesquita Filho" – UNESP/FEB
Departamento de Engenharia Mecânica
CEP. 17033-360, Bauru, SP, Brasil

Received: February 01, 2017
Revised: April 30, 2017
Accepted: May 31, 2017

ABSTRACT

Laminar forced convection inside a square cavity with inlet and outlet ports was numerically analyzed. The positions of the inlet and outlet ports were fixed and the ports sizes were equal 25% of the side wall. The influence of the Reynolds and Prandtl numbers on the flow and temperature fields inside the cavity was verified for nine cases, with Re = 50, 100 and 500 and Pr = 0.7, 3 and 5. The heat transfer process in the cavity was analyzed from obtained values for the average Nusselt number and the local Nusselt number on the walls. The open source computer package OpenFOAM® was used for simulations considering a two-dimensional flow. For all tested Prandtl numbers, there is a growth in the rotating vortex regions as Reynolds number is increases. The temperature fields are directly related to the presence of the rotating vortices and the temperature gradient is more noticeable at the interface sections of the throughflow stream with the neighboring vortices and the next to the walls for greater Reynolds and Prandtl numbers. It was verified that the local Nusselt number on the walls varies radically with minimum and maximum points and it is dependent on the flow and temperature fields adjacent to the respective wall. The results for average Nusselt number per wall indicated that the bottom wall is the most susceptible to variations in its average Nusselt number and that the top wall present higher values of this parameter for all tested cases. Finally, the average Nusselt number was increased with increasing the Reynolds and Prandtl numbers indicating the enhanced thermal exchange.

Keywords: thermal energy, ventilated cavity, numerical analysis, simulation, OpenFOAM®.

NOMENCLATURE

H	height of cavity, m
L	length of cavity, m
n	normal direction to each wall
Nu_i	local Nusselt number
$\overline{Nu}$	average Nusselt number
$\overline{Nu}_i$	average Nusselt number per wall
p	pressure, N/m^2
P	dimensionless pressure
Pr	Prandtl number, ν/α
Re	Reynolds number, $u_{in}H/\nu$
S	specific coordinate system along the walls
T	temperature, K
u, v	velocity components, m/s
U, V	dimensionless velocity components
W	dimensionless ports size
x, y, z	cartesian coordinates, m
X, Y, Z	dimensionless cartesian coordinates

Greek symbols

α	thermal diffusivity, m^2/s
θ	dimensionless temperature
ν	fluid kinematic viscosity, m^2/s
ρ	density, kg/m^3

Subscripts

i	left, bottom, right or top wall (A, B, C or D)
in	inlet
tot	total
w	wall

INTRODUCTION

The study of fluid flow and heat transfer processes inside the cavities aims different applications in engineering. The simplicity of cavity geometry enables testing and validation computer codes used for a considerable range of practical problems such as flows, heat exchangers, lubrication technology, drying technology, electronics cooling, ventilation of rooms and solar energy storage. Moreover, flow analysis in the cavities provide for researchers opportunities to investigate problems with a complex flow regime and recirculation.

The range of problems that can be analyzed with cavities is mainly related to the geometric configuration of the cavity and the type of convective flow: natural, forced or mixed. Generally, the geometric cavity configuration encompasses aspects such as: closed or open cavity, number of openings and its aspect ratio.

In recent decades, some researchers have developed works focusing on mixed convection in cavities with openings mass flow, commonly called ventilated cavities. For example, general works about mixed convection in ventilated cavities include those

of Guo and Sharif (2004), Saha et al. (2006), Khanafer et al. (2007), Saha at al. (2007), Basak et al. (2009), Cheng (2011) and Zhao et al. (2011). Others researchers have investigated the mixed convection in ventilated cavities with nanofluids, among them Mahmoudi et al. (2010), Sourtiji et al. (2011a) and Sourtiji et al. (2014).

Studies about mixed convection in ventilated cavities with any heat source or some kind of obstacle were carried out by Hsu and Wang (2000), Shuja et al. (2000), Radhakrishnan et al. (2007), Rahman et al. (2008), Ghasemi and Aminossadati (2008), Rahman et al. (2012) and Belmiloud and Sad chemloul (2015), which are related to applications in electronic cooling and ventilation of buildings.

Pure forced convection in ventilated cavities has been less explored. In more recent works, two can be highlighted in the study of forced convection in ventilated cavity, Saeidi and Khodadadi (2006) and Sourtiji et al. (2011b). Both analyzed the forced convection in a square ventilated cavity for different positions of outlet port. However, the first authors investigated the laminar forced convection inside the cavity and the second authors the turbulent forced convection. These analyses were carried out with dimensionless parameters and the influence of Reynolds number and ports size on the flow and temperature fields was verified for the same fixed Prandtl number.

The present work focuses on numerical analysis of laminar forced convection inside a specified square ventilated cavity for different Reynolds and Prandtl numbers. The influence of the Prandtl number on the flow and temperature fields in this cavity had not been verified. The flow and temperature fields were obtained and the heat transfer process in the cavity was analyzed from calculated values for the average Nusselt number and the local Nusselt number on the walls.

PROBLEM FORMULATION

Figure 1 illustrates the schematic drawing of the two-dimensional cavity. The cavity has square geometry $(\mathrm{H}=\mathrm{L})$ and two ports: one for inlet and another for fluid outlet. The fluid flow enters into the cavity from the top port of the left wall (Wall A) and leaves it from the bottom port of the right wall (Wall C). Both ports have size *W* corresponding to 25% of the size of the walls. A specific coordinate system *S* along the walls is adopted with its origin at $\mathrm{x}=0$ and $\mathrm{y}=\mathrm{H}$, as identified by the dashed lines in Fig. 1. This coordinate system corresponds to traversing the inner wall of the cavity in the counter-clockwise direction starting at the top left corner. The four walls of the cavity are maintained at a constant temperature T_w, while the inlet fluid temperature T_{in} is kept constant with $\mathrm{T_{in}} < \mathrm{T_w}$. The flow is assumed to be steady, laminar and incompressible. The fluid is Newtonian. It is negligible the effect of viscous dissipation. The fluid thermophysical properties are constant.

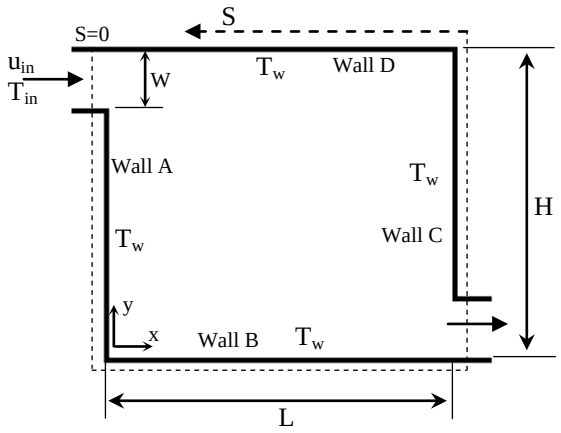

Figure 1. Schematic drawing of cavity with inlet and outlet ports.

For the foregoing considerations, the transport equations can be written in nondimensional form from the introduction of dimensionless variables, as follows:

$$X=\frac{x}{H}\;;\quad Y=\frac{y}{H};\quad U=\frac{u}{u_{in}};\quad V=\frac{v}{u_{in}};$$
$$P=\frac{p}{\rho u_{in}^2}\;;\quad \theta=\frac{T-T_{in}}{T_w-T_{in}} \tag{1}$$

where *u* and *v* are the velocity components in the Cartesian coordinate system (x-y). Variables *p* and *T* are pressure and temperature, respectively. Based on the dimensionless parameters, the transport equations for mass, momentum and energy are:

$$\frac{\partial U}{\partial X}+\frac{\partial V}{\partial Y}=0 \tag{2}$$

$$U\frac{\partial U}{\partial X}+V\frac{\partial U}{\partial Y}=-\frac{\partial P}{\partial X}+\frac{1}{\mathrm{Re}}\left[\frac{\partial^2 U}{\partial X^2}+\frac{\partial^2 U}{\partial Y^2}\right] \tag{3}$$

$$U\frac{\partial V}{\partial X}+V\frac{\partial V}{\partial Y}=-\frac{\partial P}{\partial Y}+\frac{1}{\mathrm{Re}}\left[\frac{\partial^2 V}{\partial X^2}+\frac{\partial^2 V}{\partial Y^2}\right] \tag{4}$$

$$U\frac{\partial \theta}{\partial X}+V\frac{\partial \theta}{\partial Y}=\frac{1}{\mathrm{Re}\,\mathrm{Pr}}\left[\frac{\partial^2 \theta}{\partial X^2}+\frac{\partial^2 \theta}{\partial Y^2}\right] \tag{5}$$

where the parameters *Re* and *Pr* are Reynolds number and Prandtl number, respectively.

The dimensionless boundary conditions of the problem were established as follows:

Inlet Port:

$$U = 1 \;;\quad V = 0;\quad \theta = 0 \tag{6}$$

Outlet Port:

$$\frac{\partial U}{\partial X} = 0;\qquad \frac{\partial \theta}{\partial X} = 0 \tag{7}$$

Walls:

$$U = V = 0;\quad \theta = 1 \tag{8}$$

The heat transfer rate along the walls was locally evaluated from the variations of the local Nusselt numbers defined as follow:

$$Nu_i = -\frac{\partial \theta}{\partial n}\bigg|_{wall} \tag{9}$$

where the subscript *i* represents to the left, bottom, right or top wall (A, B, C or D according Fig. 1) of the cavity. The variable *n* represents the normal direction to each wall $(\pm \mathrm{X}\ \mathrm{or} \pm \mathrm{Y})$. The *S* coordinate system (Fig. 1) was used to present the local Nusselt number variations on the four walls simultaneously, where the intervals $\mathrm{S} = 0-1$, $\mathrm{S} = 1-2$, $\mathrm{S} = 2-3$ and $\mathrm{S} = 3-4$ correspond, respectively, to the left, bottom, right and top wall.

The average Nusselt number $\overline{\mathrm{Nu}}$ was used to evaluate the total heat transfer rate of the cavity, being defined as the mean of the individual average Nusselt number per wall $\overline{\mathrm{Nu}}_\mathrm{i}$.

$$\overline{Nu_i} = -\frac{1}{\left(S_{i1} - S_{i2}\right)}\int_{S_{i1}}^{S_{i2}} Nu_i\, dS \tag{10}$$

$$\overline{Nu} = \sum_i \frac{\overline{Nu_i}\left(S_{i2} - S_{i1}\right)}{S_{tot}} \tag{11}$$

with S_{i1} and S_{i2} being the S-coordinates of the two ends of the ith wall.

NUMERICAL PROCEDURE

The numerical simulation of the cavity was performed using the computer package open source OpenFOAM® considering two-dimensional flow. Transport equations were solved iteratively by the finite volume method using the SIMPLE algorithm by Patankar (1980). The *upwind* scheme was used for the discretization of the convective terms and the *Gauss Linear* scheme was used for the diffusive terms. The subrelaxation parameters were used to the convergence of the velocity, pressure and temperature values. These parameters were set at 0.3, 0.7 and 0.8, respectively. The tolerance for convergence iterative procedure was adjusted as 10^{-4}, 10^{-5} and 10^{-3} for the velocity, pressure and temperature, respectively.

Mesh tests were performed to investigate the grid independence on the results. Six uniformly spaced grid sizes were tested and the variation of the average Nusselt number inside the cavity was observed. Table 1 present the result of grid independence for $\mathrm{Re} = 500$ and $\mathrm{Pr} = 5$.

Table 1. Result of grid independence for $\mathrm{Re} = 500$ and $\mathrm{Pr} = 5$.

Number of grids (X-Y)	$\overline{\mathrm{Nu}}$
40 x 40	24.05
80 x 80	22.47
120 x 120	21.04
160 x 160	20.07
200 x 200	19.50
240 x 240	19.20

The result of grid independence showed that the 160 x 160 grid system presented good relationship between computational simulation time and reliable results. This grid system was adopted for cavity simulation.

The variation of other parameters was also observed in the grid independence analysis, as the velocity components (U and V) and the temperature profiles along the central lines inside the cavity. All these profiles observed for the adopted grid are in good agreement when compared with those obtained with most refined grid. The greatest differences observed between the velocity components were around 10% for some punctual values. In the case for temperature profiles, the greatest variation between temperature values in the tested positions was less than 5%.

In order to validate the computational code, the laminar forced convection problem in this ventilated cavity was tested for three different Reynolds numbers and $\mathrm{Pr} = 5$. The average Nusselt number was calculated and the results were compared with those obtained by Saeidi and Khodadadi (2006). This comparison revealed good agreements between results which are show in Table 2.

Table 2. Comparison of the present study with those of Saeidi and Khodadadi (2006) for $\mathrm{Pr} = 5$.

Re	$\overline{\mathrm{Nu}}$		Difference
	Present Study	Saeidi and Khodadadi (2006)*	
40	6.35	6.80	0.066
100	9.19	9.60	0.043
500	20.07	19.80	0.013

* Estimated values from graphics of authors.

For another test validation, Sourtiji et al. (2014) present graphical results of average Nusselt number for these same cases simulated by Saeidi and Khodadadi (2006). The results present by Sourtiji et al. (2014) are very close with those obtained by

Saeidi and Khodadadi (2006).

RESULTS AND DISCUSSION

Cavity simulations were performed for nine different cases obtained from the variation of the Reynolds and Prandtl numbers. The Reynolds numbers are 50, 100 and 500. The Prandtl numbers are 0.7, 3 and 5. In all cases the inlet temperature and also the walls temperature were kept constant, with $\theta_{in} = 0$ and $\theta_w = 1$. The inlet velocity was kept constant $U_{in} = 1$ for the tested cases.

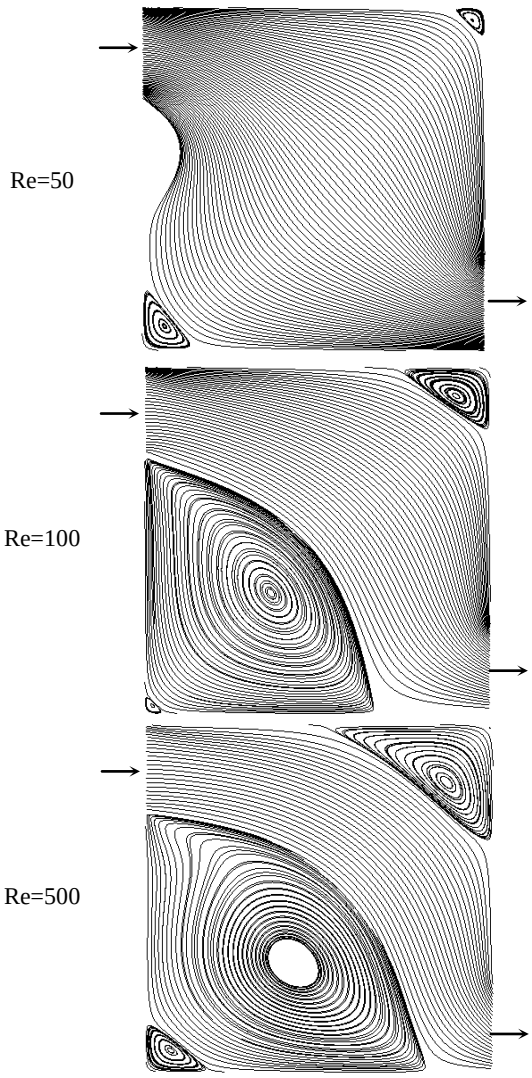

Figure 2. Streamlines for $Pr = 5$ and $Re = 50$, $Re = 100$ and $Re = 500$.

Flow fields in the cavity are represented by streamlines show in Fig. 2 for $Pr = 5$ and $Re = 50$, 100 and 500. It is observed that the streamlines have defined trajectories between the inlet and outlet ports, occupying about 90% of the cavity for $Re = 50$. A primary clockwise rotating vortex that occupies about 8% of the cavity is observed in the bottom left corner for this case. Besides, a small counter-clockwise rotating vortex is located at the top right corner of the cavity. For $Re = 100$, it is noticed an evolution of the primary clockwise rotating vortex, which occupies more than 40% of the cavity. The counter-clockwise rotating vortex located at the top right corner also increases significantly when compared with case for $Re = 50$. In addition, a very small counter-clockwise rotating vortex arises in the bottom left corner. For $Re = 500$ there is an increase of the primary clockwise rotating vortex and an even greater percentage increase of the two counter-clockwise rotating vortex when compared with case for $Re = 100$.

The results presented in Fig. 2 clearly show that increasing the Reynolds number implies in increasing the internal area of the cavity with rotating vortex. Similar results to the Fig. 2 were observed for the cases of $Pr = 0.7$ and $Pr = 3$ with $Re = 50$, 100 and 500.

Figure 3 shows the velocity fields for $Pr = 5$ and $Re = 50$, 100 and 500. It is observed for the three cases that the higher velocity components are present in the throughflow stream region comprised between the inlet and outlet ports of the cavity. In this figure, it is also possible to note that with the increase Reynolds number, there is an increase of regions inside the cavity with a significant decrease of the velocity component due to the growth of rotating vortex regions. Smaller velocity components appear in the rotating vortex regions, especially in the cavity bottom left corner for each case. Another aspect is that the highest values of the magnitude velocity components shown in each case are close to each other: $U = 1.37$ for $Re = 50$, $U = 1.40$ for $Re = 100$ and $U = 1.54$ for $Re = 500$.

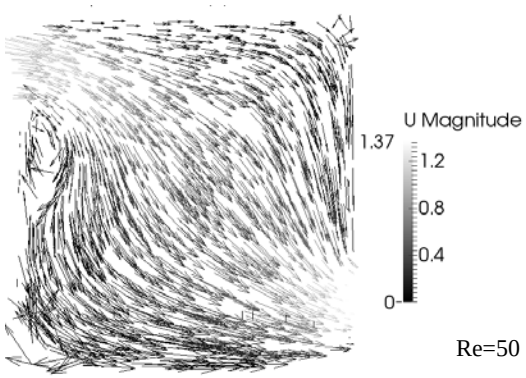

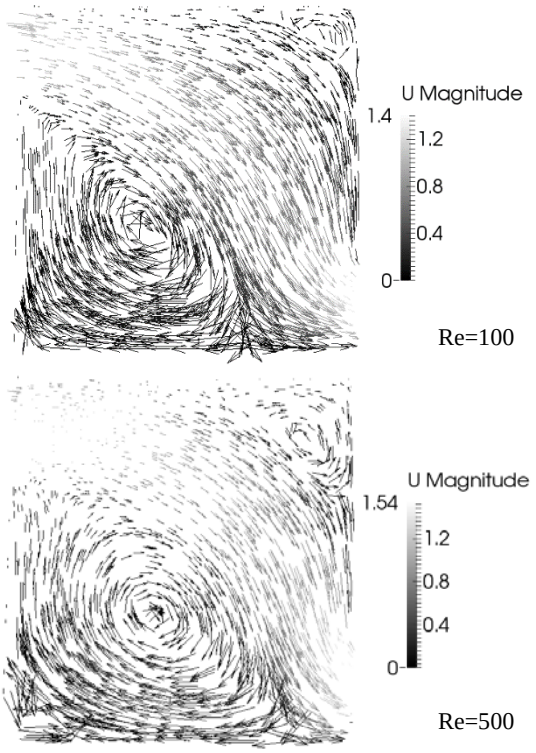

Figure 3. Velocity fields for $\mathrm{Pr}=5$ and $\mathrm{Re}=50$, $\mathrm{Re}=100$ and $\mathrm{Re}=500$.

Figure 4 show the contours (isotherms) of dimensionless temperature corresponding to nine cases tested in this study. It is observed for $\mathrm{Re}=50$ and $\mathrm{Pr}=0.7$ that the fluid temperature exhibit moderate spatial variations inside the cavity, except next to inlet region. The fluid temperature gradients are marked next to the top portion of the left wall. When Prandtl number increases $(\mathrm{Pr}=3)$, it is noticed that the fluid temperature exhibit less moderate spatial variations inside the cavity and the fluid temperature gradients are marked next to inlet and outlet regions. For $\mathrm{Pr}=5$, the marked temperature gradients are intensified next to inlet and outlet regions. A similar behavior is observed when Reynolds number increases to $\mathrm{Re}=100$. It is observed that the fluid temperature gradients are marked next to the top left corner, next to the right side of bottom wall and next to the bottom portion of the right wall. These marked temperature gradients intensifies with increasing Prandtl number. In additional, in this case, the fluid temperature exhibit less moderate spatial variations inside the cavity when compared to $\mathrm{Re}=50$. It is noted that the increasing of Reynolds number causes more steeper fluid temperature gradients in the central region of the cavity. For $\mathrm{Re}=500$, the marked temperature gradients are more expressive and they became more intense with increasing Prandtl number, especially next to walls and the inlet region.

The temperature fields showed in Fig. 4 are related to the flow fields in the cavity. An analysis in the case of $\mathrm{Re}=500$ indicates that the temperature gradient is marked at the interface sections of the throughflow stream and the clockwise rotating primary vortex, suggesting significantly heat exchange from the incoming fluid to the clockwise primary vortex. As Prandtl number increases, it is noticed that the temperature gradient is also marked at the interface sections of the throughflow stream and the counter-clockwise rotating vortex located at the top right corner of the cavity.

Finally, the cases shown in Fig .4 indicate that the regions of intense fluid temperature gradients are found on both sides of the inlet and outlet ports, except for the case with $\mathrm{Re}=50$ and $\mathrm{Pr}=0.7$, in which it is not observed at the outlet port. For the highest Reynolds and Prandtl numbers, marked temperature gradients are clearly noted on both sides of the throughflow stream indicating intense heat exchange with the neighboring vortices.

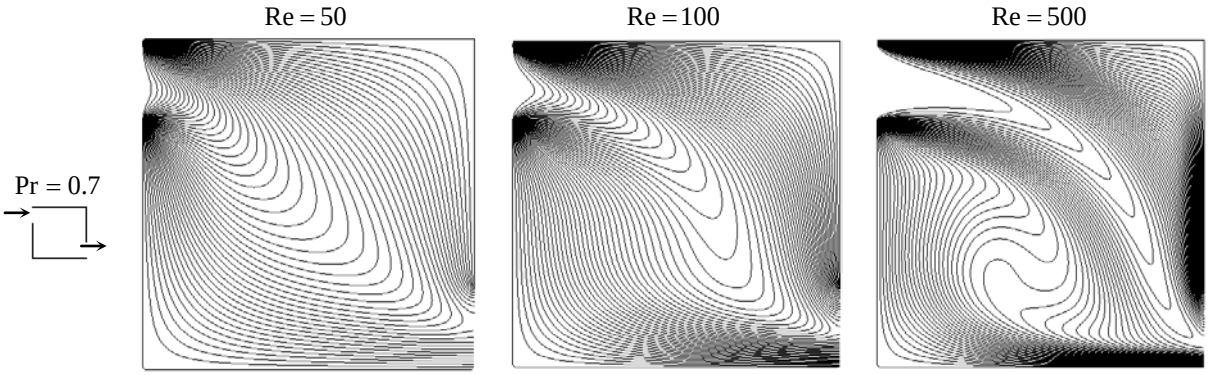

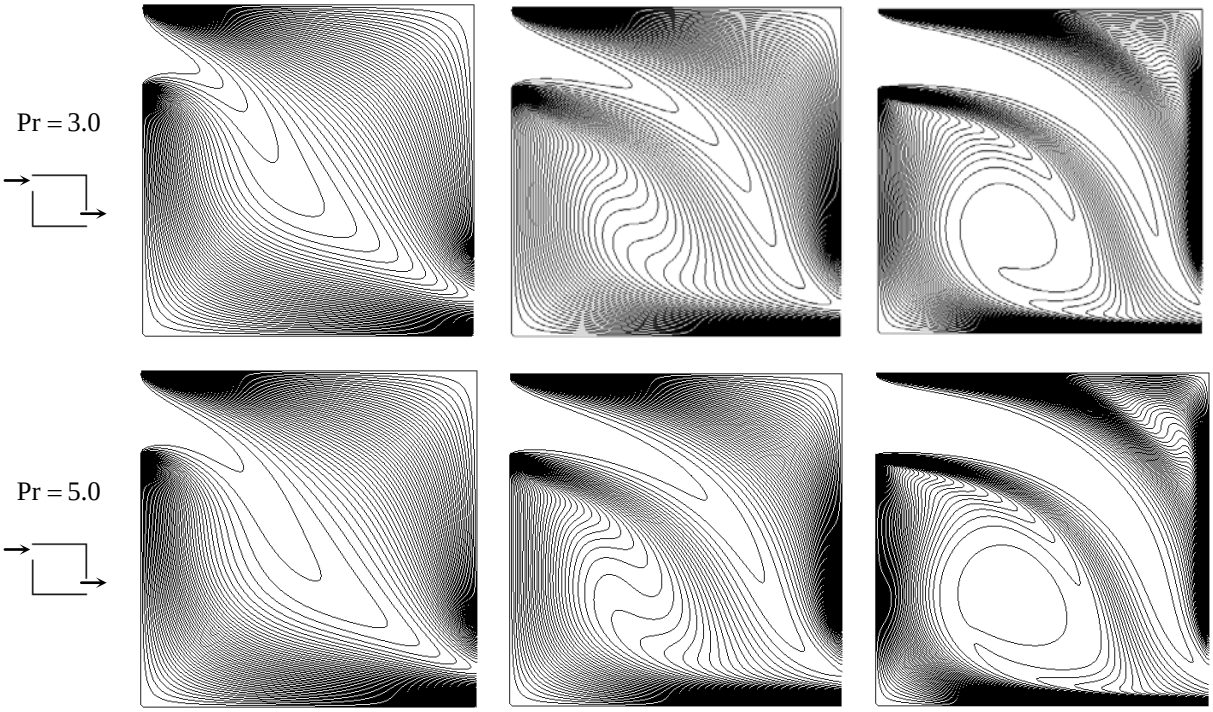

Figure 4. Temperature fields for Reynolds numbers of 50, 100 and 500 and Prandtl numbers of 0.7, 3 and 5.

Variations of the local Nusselt number on the four walls of the cavity are show in Fig. 5. The local Nusselt number distribution along four walls is presented in graphics for fixed Reynolds number (50, 100 and 500) and Prandtl numbers of 0.7, 3 and 5 for each Reynolds. In this figure, no data for the Nusselt number is shown for $S = 0 - 0.25$ that corresponds to the location of the inlet port. Discontinuities for each individual curve correspond to the location of the outlet port. These Nusselt numbers correspond to the temperature fields shown in Fig. 4 and are directly affected by those variations.

It is observed that the local Nusselt values are higher on the both sides of the inlet and outlet ports indicating intense heat exchange rate due to temperature gradient already explained in Fig. 4. The corners $(S = 1 \text{ and } 3)$ of the cavity that are not next to the ports have very poor heat transfer rate due to the slow motion of the fluid in these regions. There is also a monotonic variation of the local Nusselt number, with rise and decline, between the two extreme rates of heat transfer.

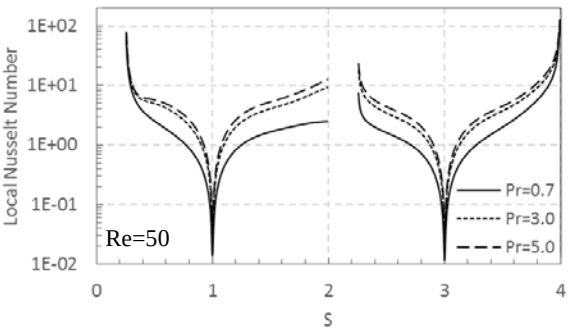

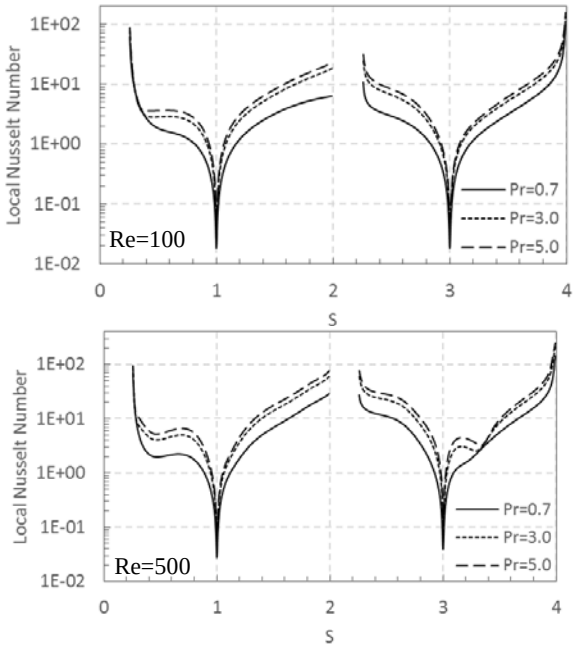

Figure 5. Local Nusselt number distribution along four walls of the cavity for different Reynolds and Prandtl numbers.

Besides, for a fixed Reynolds number, as the Prandtl number increases, the local Nusselt number rises due to the augmenting of the heat exchange in the cavity. The increase of Reynolds number, for the same Prandtl number, also implies the increase of Local Nusselt number in the cavity.

The average Nusselt number of the cavity can also be used to evaluate the heat transfer rate inside the cavity. Table 3 show the average Nusselt number

for $Re = 50$, 100 and 500 and $Pr = 0.7$, 3 and 5. It is observed that for a given Reynolds number, the average Nusselt number increases with increasing Prandtl number. Otherwise, for a given Prandtl number, the average Nusselt number increases with increasing Reynolds number, indicating an increase in the thermal exchange.

Table 3. Average Nusselt numbers for different Reynolds and Prandtl numbers.

Re	$\overline{Nu}$		
	$Pr = 0.7$	$Pr = 3.0$	$Pr = 5.0$
50	3.16	5.53	6.65
100	4.23	7.42	9.19
500	8.69	16.00	20.07

Table 3 clearly shows that increasing the Reynolds number as well as the Prandtl number implies in the enhanced thermal exchange inside the cavity. An analysis in the results of Tab. 3 shows that increasing the Reynolds number from 50 to 100 implies an increase of about 35% in the average Nusselt number for the three tested Prandtl numbers. This percentage is greater than 100% when Reynolds number increases from 100 to 500.

Another variable utilized to evaluate the heat transfer rate is the average Nusselt number per wall of the cavity. Figure 6 shows the variation of the average Nusselt number per wall for fixed Reynolds number (50, 100 and 500) and Prandtl numbers of 0.7, 3 and 5 for each Reynolds.

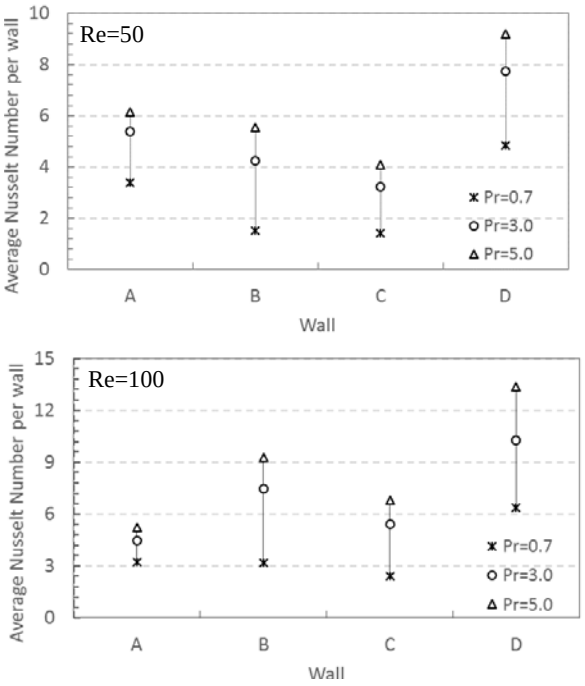

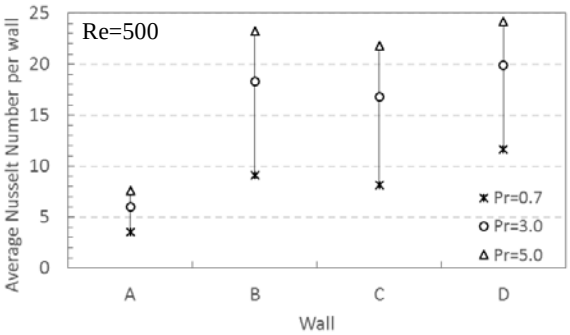

Figure 6. Variation of the average Nusselt number per wall of the cavity for different Reynolds and Prandtl numbers.

These results are interesting because they show the behavior of the thermal exchange in each wall for the tested cases. It is noted that for the three tested Reynolds numbers, the walls C (right) and D (top) have practically the same percentage increase in the average Nusselt number between the values of $Pr = 0.7$ and $Pr = 5.0$. This increase was about 2.8 times in wall C and 2 times in wall D. For wall A (left) a similar percentage increase of average Nusselt number (about 1.7 times) is observed between $Pr = 0.7$ and $Pr = 5.0$ for the cases with $Re = 50$ and $Re = 100$. This increase was about 2 times in wall A for $Re = 500$. Wall B (bottom) presented different variations of the average Nusselt number between $Pr = 0.7$ and $Pr = 5.0$ for the three different tested Reynolds numbers. These variations were around 3.6 times for $Re = 50$, 2.9 times for $Re = 100$ and 2.5 times for $Re = 500$.

Thus, these results indicate that the wall B of the cavity studied in this work is the most susceptible to variations in its average Nusselt number, considering a specified interval for the Prandtl numbers and different Reynolds numbers.

Still on Fig. 6, the wall D present the higher values of average Nusselt when compared with the values of other walls, considering the same Prandtl number for each tested Reynolds number. Other aspect is that the average Nusselt number for wall A are greater than those of wall C for $Re = 50$. As Reynolds number increases, the average Nusselt numbers for wall C increase until they override the values of average Nusselt for wall A, as can be seen clearly in the graph for $Re = 500$. So, for $Re = 50$, the wall A exchanges more heat with the fluid than the wall C. For $Re = 500$ the opposite occurs. This characteristic is consistent with the temperature gradients shown in the Fig. 4.

CONCLUSIONS

In this work, a square ventilated cavity subjected to forced laminar convection have been investigated numerically. Nine different cases were simulated from the variation of the Reynolds and Prandtl numbers and the effects of these governing

parameters on the characteristics of the flow and thermal fields were analyzed.

An analysis of the flow fields in the cavity revealed that, for all tested Prandtl numbers, there is a growth in the rotating vortex regions as Reynolds number is increases. Rotating vortices covered about 10% of the cavity for the smallest tested Reynolds number and about 70% for the largest tested Reynolds number. Besides, the velocity fields inside the cavity showed that smaller velocity components appear in the rotating vortex regions, especially in the left bottom corner of the cavity.

The temperature fields are directly related to the presence of the rotating vortices inside the cavity. Temperature gradient is more noticeable at the interface sections of the throughflow stream with the neighboring vortices and the next to the walls for greater Reynolds and Prandtl numbers, suggesting significantly heat exchange in these regions. The increase of Reynolds and Prandtl numbers intensifies these temperature gradients.

The local Nusselt number varies radically with minimum and maximum points and it is dependent on the flow and temperature fields adjacent to the respective wall. The minimum points occur in the corners of the cavity where there are no ports and the maximum points occur next to the inlet and outlet ports. It was also verified that the local Nusselt number is increased with increasing the Reynolds and Prandtl numbers.

The average Nusselt number is also increased with increasing the Reynolds and Prandtl numbers indicating the enhanced thermal exchange. The average Nusselt number per wall showed the behavior of the thermal exchange in each wall for the tested cases. The results indicated that the bottom wall is the most susceptible to variations in its average Nusselt number and consequently, to its rate of heat exchanged with the fluid. Furthermore, the top wall is the one that presents the greatest thermal exchange with the fluid for all tested cases.

REFERENCES

Basak, T., Roy, S., Sharma, P. K., and Pop, I., 2009, Analysis of Mixed Convection flows within a Square Cavity with Uniform and Non-Uniform Heating of Bottom Wall, International Journal of Thermal Sciences, Vol. 48, pp. 891-912.

Belmiloud, M. A., and Sad Chemloul, N., 2015, Effect of Baffle Number on Mixed Convection within a Ventilated Cavity, Journal of Mechanical Science and Technology, Vol. 29, No. 11, pp. 4719-4727.

Cheng, T. S., 2011, Characteristics of Mixed Convection Heat Transfer in a Lid-Driven Square Cavity with various Richardson and Prandtl Numbers, International Journal of Thermal Sciences, Vol. 50, pp. 197-205.

Ghasemi, B., and Aminossadati, S. M., 2008, Numerical Simulation of Mixed Convection in a Rectangular Enclosure with Different Numbers and Arrangements of Discrete Heat Sources, Arabian Journal for Science and Engineering, Vol. 33, No. 1B, pp. 189-207.

Guo, G., and Sharif, M. A. R., 2004, Mixed Convection in Rectangular Cavities at Various Aspect Ratios with Moving Isothermal Sidewalls and Constant Flux Heat Source on the Bottom Wall, International Journal of Thermal Science, Vol. 43, pp. 465-475.

Hsu, T. H., and Wang, S. G., 2000, Mixed Convection in a Rectangular Enclosure with Discrete Heat Sources, Numerical Heat Transfer, Part A, Vol. 38, pp. 627-652.

Khanafer, K. M., Al-Amiri, A. M., and Pop, I., 2007, Numerical Simulation of Unsteady Mixed Convection in a Driven Cavity using an Externally Excited Sliding Lid, Eur. J. Mech. B/Fluids, Vol. 26, pp. 669-687.

Mahmoudi, A. H., Shahi, M., and Talebi, F., 2010, Effect of inlet and outlet Location on the Mixed Convective Cooling Inside the Ventilated Cavity Subjected to an External Nanofluid, International Communications in Heat and Mass Transfer, Vol. 37, pp. 1158-1173.

Patankar, S. V., 1980, *Numerical Heat Transfer and Fluid Flow*, Hemisphere, New York.

Radhakrishnan, T. V., Verma, A. K., Balaji, C., and Venkateshan, S. P., 2007, An Experimental and Numerical Investigation of Mixed Convection from a Heat Generating Element in a Ventilated Cavity, Experimental Thermal and Fluid Science, Vol. 32, pp. 502-520.

Rahman, M. D. M., Alim, M. A., Saha, S., and Chowdhury, M. K., 2008, A Numerical Study of Mixed Convection in a Square Cavity with a Heat Conducting Square Cylinder at Different Locations, Journal of Mechanical Engineering, Vol. 39, No. 2, pp. 78-85.

Rahman, M. M., Parvin, S., Rahim, N. A., Islam, M. R., Saidur, R., and Hasanuzzaman, M., 2012, Effects of Reynolds and Prandtl Number on Mixed Convection in a Ventilated Cavity with a Heat-Generating Solid Circular Block, Applied Mathematical Modelling, Vol. 36, pp. 2056-2066.

Saeidi, S. M., and Khodadadi, J. M., 2006, Forced Convection in a Square Cavity with inlet and outlet Ports, International Journal of Heat and Mass Transfer, Vol. 49, pp. 1896-1906.

Saha, S., Saha, G., Ali, M., and Islam, Md. Q., 2006, Combined Free and Forced Convection inside a Two-Dimensional Multiple Ventilated Rectangular Enclosure, ARPN Journal of Engineering and Applied Sciences, Vol. 1 No. 3, pp. 23-35.

Saha, S., Saha, G., Ali, M., and Islam, Md. Q., 2007, Combined Free and Forced Convection inside a Two-Dimensional Multiple Ventilated Rectangular Enclosure, ARPN Journal of Engineering and Applied Sciences, Vol. 2 No. 2, pp. 25-36.

Shuja, S. Z., Yibas, B. S., and Iqbal, M. O., 2000, Mixed Convection in a Square Cavity Due to Heat Generating Rectangular Body. Effect of Cavity exit Port Locations, International Journal of Numerical Methods for Heat & Fluid Flow, Vol. 10, pp. 824-841.

Sourtiji, E., Gorji-Bandpy, M., Ganji, D. D., and Hosseinizadeh, S. F., 2014, Numerical Analysis of Mixed Convection Heat Transfer of Al2O3-Water Nanofluid in a Ventilated Cavity Considering Different Positions of the Outlet Port, Powder Technology, Vol. 262, pp. 71-81.

Sourtiji, E., Hosseinizadeh, S. F., Gorji-Bandpy, M., and Ganji, D. D., 2011a, Effect of Water-Based Al2O3 Nanofluids on Heat Transfer and Pressure Drop in Periodic Mixed Convection Inside a Square Ventilated Cavity, International Communications in Heat and Mass Transfer, Vol. 38, pp. 1125-1134.

Sourtiji, E., Hosseinizadeh, S. F., Gorji-Bandpy, M., and Khodadadi, J. M., 2011b, Computational Study of Turbulent Forced Convection Flow in a Square Cavity with Ventilation Ports, Numerical Heat Transfer, Part A, Vol. 59, Issue 12, pp. 954-969.

Zhao, M., Yang, M., Lu, M., and Zhang, Y., 2011, Evolution to Chaotic Mixed Convection in a Multiple Ventilated Cavity, International Journal of Thermal Sciences, Vol. 50, pp. 2464-2472.